KTH Chemical Science and Engineering

Performance of Conventional and Structural Lithium-Ion Batteries

Maria Hellqvist Kjell

Doctoral Thesis

Applied Electrochemistry, School of Chemical Science and Engineering
Kungliga Tekniska Högskolan, Stockholm 2013

Akademisk avhandling som med tillstånd av Kungliga Tekniska högskolan i Stockholm, framlägges till offentlig granskning för avläggande av teknologie doktorsexamen onsdagen den 12 juni 2013, kl.10.00 i sal K2, Teknikringen 28, KTH

Printed in Sweden
E-Print, Stockholm 2013

TRITA-CHE Report 2013:28
ISSN 1654-1081
ISBN 978-91-7501-774-7

“Don’t panic”

- Hitchhiker’s Guide to the Galaxy, Douglas Adams

Abstract

Lithium-ion batteries have, in recent years, experienced a rapid development from small everyday devices towards hybrid electric vehicle (HEV) applications. Due to this shift in application area, the battery performance and its degradation with time are becoming increasingly important issues to be solved.

In this thesis, lithium-ion batteries are investigated with focus on lifetime performance of an existing battery chemistry, and development of electrodes for so-called structural batteries. The systems are evaluated by electrochemical methods, such as cycling and electrochemical impedance spectroscopy (EIS), combined with material characterization and modeling.

Lifetime performance of mesocarbon microbeads (MCMB)/$LiFePO_4$ cells was investigated to develop an understanding of how this technology tolerates and is influenced by different conditions, such as cycling, storage and temperature. The lifetime of the $LiFePO_4$-based cells was found to be significantly reduced by cycling at elevated temperature, almost five times shorter compared to cycle-aged cells at ambient temperature. The calendar-aged cells also showed major signs of degradation at elevated temperatures. The overall cause of aging was electrolyte decomposition which resulted in loss of cyclable lithium, i.e. capacity fade, and impedance increase.

Commercially available polyacrylonitrile (PAN)-based carbon fibers were investigated, both electrochemically and mechanically, to determine their suitability as negative electrodes in structural batteries. The electrochemical performance of carbon fibers was found to be excellent compared to other negative electrode materials, especially for single or well-separated fibers. The mechanical properties, measured as changes in the tensile properties, showed that the tensile stiffness was unaffected by lithium-ion intercalation and cycling. The ultimate tensile strength, however, showed a distinct variation with state-of-charge (SOC). Overall, carbon fibers are suitable for structural-battery applications.

Key words: aging, carbon fibers, $LiFePO_4$, lifetime performance, lithium-ion batteries, multifunctional materials, structural batteries

Sammanfattning

Utvecklingen av litiumjonbatterier har de senaste åren tilltagit eftersom nya användningsområden såsom hybrid- och elbilar nu blivit aktuella. För att batterierna ska klara de påfrestningar en sådan förändring medför behöver man förbättra prestandan samt öka livslängden.

I denna avhandling har litiumjonbatterier studerats med fokus på livslängd för en existerande batterikemi samt utveckling av elektroder för så kallade strukturella batterier. Systemen utvärderades elektrokemiskt m.h.a. cykling och impedansspektroskopi kombinerat med materialkarakterisering och modellering.

Celler baserade på ”mesocarbon microbeads” (MCMB)/$LiFePO_4$ studerades för att utvärdera vilken påverkan olika faktorer såsom cykling, lagring och temperatur har på livslängden för just denna kemi. Resultaten visade att cykling vid hög temperatur förkortade livstiden väsentligt, den blev nästan fem gånger kortare än för cykling vid rumstemperatur. Vid hög temperatur uppvisade även de kalenderåldrade cellerna tecken på prestandadegradering. Den generella orsaken till åldring var nedbrytning av elektrolyten som resulterade i förlust av cyklingsbart litium, d.v.s. kapacitetsförlust och en ökning av cellimpedansen.

Kommersiella PAN-baserade kolfibrer studerades, både elektrokemiskt och mekaniskt, för att avgöra deras lämplighet som negativa elektroder i strukturella batterier. Den elektrokemiska prestandan hos de testade kolfibrerna visade sig vara mycket god speciellt för enskilda fibrer jämfört med andra elektrodmaterial. Dragstyvheten hos fibrerna uppvisade ingen påverkan från interkalation av litiumjoner. Draghållfastheten däremot visade en tydlig variation med laddningstillståndet hos fibrerna. Den generella slutsatsen från dessa studier är att kolfiber kan anses mycket lämpliga för användning i strukturella batterier.

List of Papers

This thesis is a summary of the following papers, appended at the end, and some additional unpublished results.

Paper I Comparing aging of MCMB graphite/$LiFePO_4$ cells at 22 °C and 55 °C – Electrochemical and photoelectron spectroscopy studies. M. H. Kjell, S. Malmgren, K. Ciosek, M. Behm, K. Edström, G. Lindbergh. *Manuscript under revision after peer review in Journal of Power Sources*

Paper II Aging in lithium-ion batteries: Model and experimental investigation of harvested $LiFePO_4$ and MCMB graphite electrodes. T. G. Zavalis, M. Klett, M. H. Kjell, M. Behm, R. W. Lindström, G. Lindbergh. *Accepted for publication in Electrochimica Acta*

Paper III PAN-Based carbon fiber negative electrodes for structural lithium-ion batteries. M. H. Kjell, E. Jacques, D. Zenkert, M. Behm, G. Lindbergh. *Journal of the Electrochemical Society*, **158** (12), A1455-A1460 (2011)

Paper IV Characterization of lithium intercalation processes of PAN-based carbon fibers in a microelectrode system. M. H. Kjell, T. G. Zavalis, M. Behm, G. Lindbergh. *Submitted to Journal of the Electrochemical Society*

Paper V Impact of electrochemical cycling on the tensile properties of carbon fibres for structural lithium-ion composite batteries. E. Jacques, M. H. Kjell, D. Zenkert, G. Lindbergh, M. Behm, M. Willgert. *Composites Science and Technology*, **72**, 792–798 (2012)

Paper VI Expansion of carbon fibres induced by lithium-ion intercalation for structural electrode applications. E. Jacques, M. H. Kjell, D. Zenkert, G. Lindbergh, M. Behm. *Carbon*, **59**, 246-254 (2013)

The material characterization with X-ray photoelectron spectroscopy (XPS) in Paper I was performed by Sara Malmgren. In Paper II, Tommy Zavalis developed the macroscopic impedance model, Matilda Klett was responsible for the three-electrode measurements, and Tommy and Matilda developed the microscopic modeling features. The full-cell correlation approach was set up together with Tommy and Matilda. The carbon-fiber specimens used in Papers III, IV, and VI were supplied by Eric Jacques who was also responsible for the tensile testing in Papers V and VI. In Paper IV, the modeling and optimization was performed by Tommy Zavalis.

The following publications, containing contributions from the author compiled during the thesis work, are not included in the thesis:

i Photoinduced free radical polymerization of thermoset lithium battery electrolytes. M. Willgert, M. H. Kjell, E. Jacques, M. Behm, G. Lindbergh, M. Johansson *European Polymer Journal,* **47**, 2372–2378 (2011)

ii Photoinduced polymerization of structural lithium-ion battery electrolytes. M. Willgert, M. H. Kjell, G. Lindbergh, M. Johansson. *Abstract of Papers of the American Chemical Society,* **241** (2011)

iii Thiol-ene systems in lithium ion conducting thermoset electrolytes. M. Willgert, M. H. Kjell, G. Lindbergh, M. Johansson. *Solid State Ionics*, **236**, 22-29 (2013)

iv Lithium-ion pouch cell integrity regarding humidity in a vehicle application. P. Svens, M. H. Kjell, C. Tengstedt, G. Flodberg, G. Lindbergh. *Energies*, **6** (1), 400-410 (2013)

v Piezoelectric and piezo-electrochemical effects in lithium-intercalated carbon fibres used as structural electrodes. E. Jacques, M. H. Kjell, D. Zenkert, G. Lindbergh. *To be submitted to Electrochemistry Communications*

Contents

Chapter 1

Introduction

At the end of the 20th century, the demand for rechargeable batteries increased due to the emerging wireless technology market. The high energy and power density of the lithium-ion battery made this growth possible and today lithium-ion batteries power all sorts of everyday portable devices such as smart phones and laptops. Lithium-ion batteries have since then experienced a rapid development fueled by the automotive industry's need for producing more fuel-efficient vehicles, such as hybrid electric vehicles (HEV), in order to reduce the dependency on non-renewable energy sources and CO_2 levels. As the applications are shifting from portable consumer electronics to vehicles, where larger power and energy demands together with an extended lifetime[1] and the possibility to operate under extreme conditions are critical[2]; performance and its degradation with time are becoming increasingly important issues to be solved.

Battery performance can be improved in several ways. A common approach is to try to find new materials with superior electrochemical properties. Minimizing the amount of inactive material (less weight impact) is another way to increase the specific energy and power in a battery. The development of new smart designs and concepts that can add other values to the battery or its application is also a viable approach. In recent years, the use of multifunctional materials has attracted more and more attention in other research areas due to the possibility of combining several properties in a single entity[3]. Structural batteries, energy storage combined with load-carrying properties, are based on the idea of multifunctionality, achieving optimization of mass and volume on a system level instead of on cell level.

A greater insight into the effects of aging on the performance over time is also needed to improve existing technologies and develop the next generation of batteries. This knowledge could also contribute to the design of battery management systems[4,5] and more reliable on-board state-of-health (SOH) indicators[6].

For a more detailed understanding of performance and its degradation with time, a toolbox combining electrochemical experiments with material characterization and physics-based electrochemical modeling is required. In this thesis, both aging in a conventional lithium-ion battery system and the development of new multifunctional electrodes for structural batteries are investigated using the above-mentioned toolbox.

1.1 Lithium-ion batteries

A lithium-ion battery cell consists of two porous composite electrodes, a positive and a negative, separated by an electrolyte, a lithium-ion conducting medium in liquid or solid form[7]. In case a liquid electrolyte is used, a porous separator is needed to prevent short circuits. Both electrodes are of the lithium-ion intercalating type, i.e. the active materials can store lithium ions in their crystal lattice. In addition to the active material (typically metal oxides or phosphates for the positive electrode and carbon for the negative), the electrodes also include a binder and, if necessary, a conductive additive. The active material and binder are coated onto current collectors, usually aluminum for the positive and copper for the negative electrode.

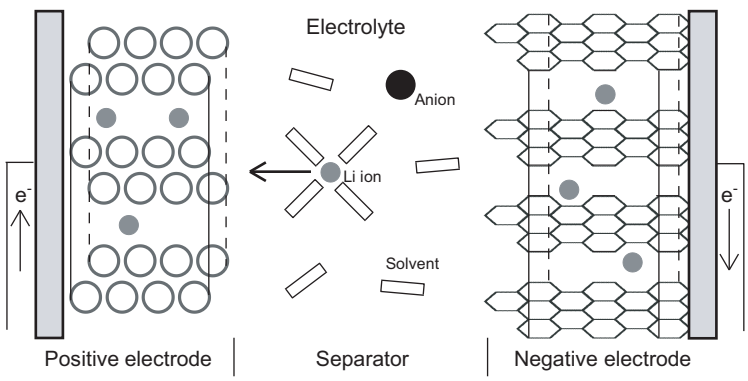

Figure 1.1 *Illustration of the working principle of a lithium-ion battery during discharge.*

The working principle is based on the transport of lithium ions from one of the electrodes through the electrolyte to the other electrode while the electrons travel through the external circuit (figure 1.1). Depending on the direction of the ions, the cell is either charged (positive to negative) or discharged (negative to positive).

1.2 Aging in lithium-ion batteries

Aging can be defined as the change in performance with time and use. One of the great challenges when working with lithium-ion batteries is to predict and diagnose aging. This is made more difficult since there are no strict guidelines on how to evaluate performance degradation and degradation in lithium-ion batteries is furthermore a relatively slow process at ambient temperature. To reduce testing time from years to months, variable conditions such as cycling at different current loads, state-of-charge (SOC), SOC window and different temperatures are often used in order to estimate lifetime. However, due to the complex nature of lithium-ion batteries identification of the factors and mechanisms behind performance degradation is challenging. In addition, depending on the application, the cause of aging can be more or less detrimental to the performance. In general, applications such as portable consumer electronics, where the battery functions as the primary energy source, are more sensitive to capacity fade than increase in cell impedance (power fade). Applications such as HEVs, on the other hand, use the battery as an energy buffer for short high-power pulses, and are therefore more sensitive to power fade than capacity fade.

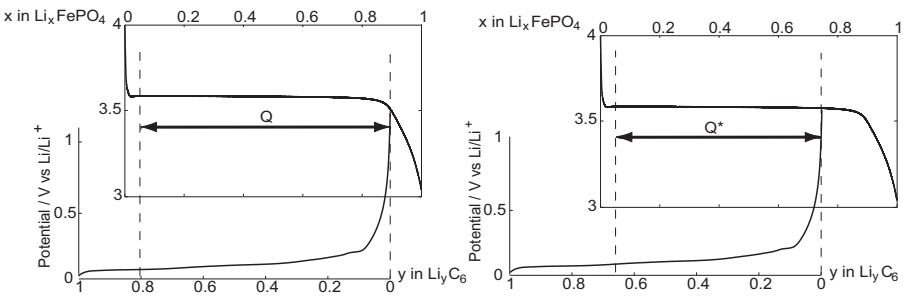

Figure 1.2 *Electrode imbalance caused by loss of cyclable lithium. Notations: Q original capacity window (left), Q* reduced capacity window (right).*

The capacity is connected to the cyclable charge available in the battery, i.e. the amount of lithium ions that can be transferred from one electrode to the other during charge or discharge. Capacity fade can develop from loss of active electrode material[8-10], or loss of lithium ions through electrolyte decomposition reactions and solid electrolyte interphase (SEI) formation[11-20]. A loss of cyclable lithium will also cause a shift between the positive and negative electrode, resulting in a smaller capacity window[16,21], as illustrated in figure 1.2. So even if all the active material in both electrodes remains the degree of utilization decreases.

Increasing cell impedance can be a result of contact losses within the porous electrodes or to the current collector, loss of active electrode material, formation of resistive surface films, and changes in electrode or separator morphology[9,22-24]. However, several of the different mechanisms mentioned above can cause both capacity fade and increased cell impedance. An overview of the basic electrode-aging mechanisms is shown in figure 1.3.

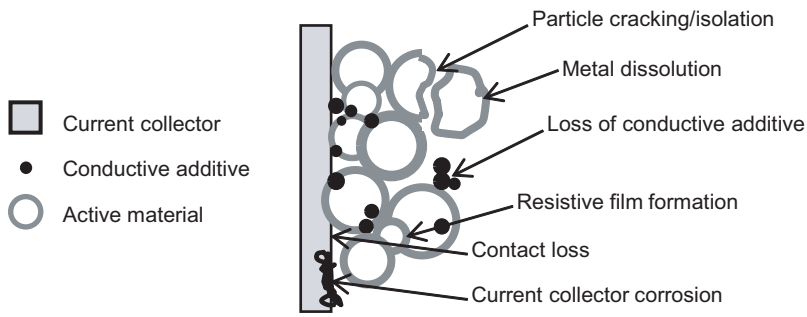

Figure 1.3 *Overview of electrode aging mechanisms.*

Graphitized carbon-based materials are the most frequently used in the negative electrode in lithium-ion batteries even though they are not electrochemically stable in the most common electrolytes. However, at the beginning of cycling an SEI is formed[25], which protects the electrode from further degradation but also causes an initial irreversible capacity loss as it consumes lithium. The thickness of the SEI should be sufficient to enable lithium intercalation into the graphite particles and prevent side reactions from taking place at the same time. A continuous growth of electrolyte decomposition products can occur, and be accelerated by exposure of fresh material[9,13], high current loads[16], metal dissolution from the positive electrode

or current collector[26-30], and elevated temperatures[9,31,32]. Deposition of electrolyte decomposition products can influence pore size and structure, electrolyte wettability, and contact resistances of the positive[23,30,33-38] and negative[9,16,17,31,38,39] electrodes, as well as the separator porosity [40-42].

High current loads have also been reported to cause cracking in the active material in the positive electrode[34,43,44], and is thought to originate in the substantial mechanical stresses created in the active material by concentration gradients[45,46]. Unlike the total particle breakup seen for many positive electrodes, the cracking of the negative electrode material is more often located on the surfaces[9,47]. Cracking is also likely to isolate active material particles from electrochemical reaction, since it causes contact losses within the electrode and to the current collector[38,43,44,48]. The mechanical stresses in the battery have also been shown to be detrimental to the polyolefin-based separators often used in commercial cells, causing pore closure[49].

Contaminants, such as water, are also responsible for aging, especially for the $LiPF_6$ salt used in lithium-ion batteries which decomposes into hydrofluoric acid in contact with water. Hydrofluoric acid is highly reactive and will damage the electrodes as well as the electrolyte. The following reactions have been proposed for the salt decomposition[50]:

$$LiPF_6 \rightleftharpoons LiF + PF_5$$

$$PF_5 + H_2O \rightarrow OPF_3 + 2HF$$

Due to the reactivity of the $LiPF_6$ salt with water, manufacturing of lithium-ion batteries requires a controlled, moisture-free, environment and packaging which will prevent moisture from penetrating the cell. Several other mechanisms have been proposed for the decomposition of the carbonate-based electrolyte solvents[19,20].

An important thing to remember is that lithium-ion batteries are a group of batteries with varying composition and that the degradation processes are connected to the specific chemistry and to the specific conditions used[9,33]. So in order to obtain an accurate assessment of the aging for a specific application, tests have to be constructed so that a suitable set of parameters is used that mirrors the right kind of conditions.

1.3 Multifunctionality in lithium-ion batteries

1.3.1 Carbon-fiber electrodes

Since lithium ions can basically be reversibly intercalated into most kind of carbons[51,52], it is possible to use continuous carbon-fiber tows as electrode material. A fiber-based electrode can be designed so that no current collectors, conductive additives or polymeric binder will be needed; the structural integrity of the electrode is given by the fibers themselves and the need for a fully covering current collector is made redundant since carbon fibers have reasonably good electrical conductivity[53,54]. These multifunctional features enable the minimization of the amount of inactive materials required to assemble a functioning negative electrode. In a conventional lithium-ion battery only one third of the theoretical specific energy remains if the weight of all the inactive components, not including the casing or protective circuitry, are accounted for, with the largest contribution from the copper current collector. In figure 1.4 a scanning electron microscope (SEM) image of a conventional negative electrode consisting of graphite powder and polymeric binder can be seen together with an image of a polyacrylonitrile (PAN)-based carbon fiber, illustrating the differences between the two kinds of electrode.

The two most commonly used precursors for commercial manufacturing of carbon fibers are pitch and PAN[55]. In general, PAN-based fibers usually exhibit higher ultimate tensile strength while pitch-based fibers often have higher tensile modulus, i.e. resistance to extension under load. However, depending on the precursor and manufacturing process, the fiber microstructure, and thus the fiber properties, will vary significantly[56]. Traditionally, the battery community has favored the pitch-based fibers as electrode material due to a higher degree of graphitization[57,58], but research has shown the disordered structure of PAN-based fibers to be more favorable for lithium-ion intercalation[59-62].

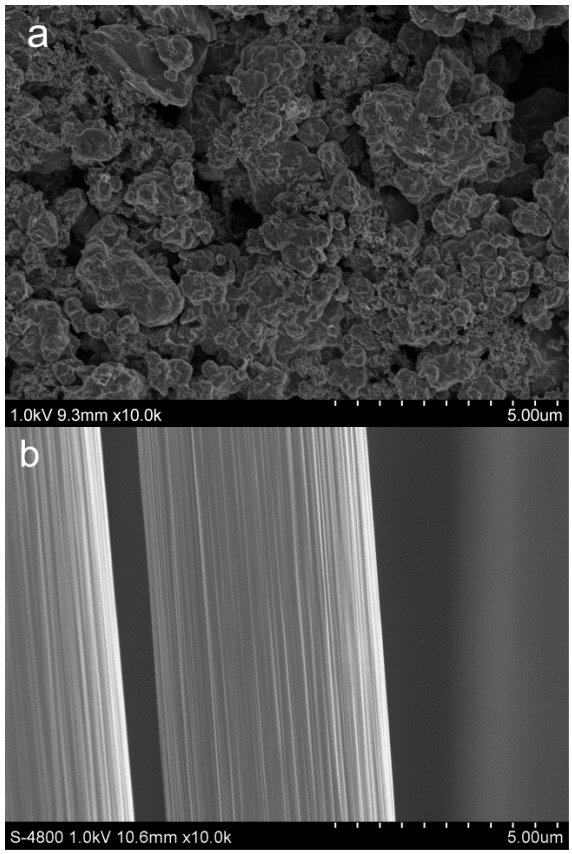

Figure 1.4 *SEM images of a) a conventional negative electrode, and b) a PAN-based carbon fiber.*

1.3.2 Structural batteries

Carbon fibers are typically used as structural reinforcement in composite materials due to their high tensile properties to weight ratio. Adding a solid polymer electrolyte (SPE) instead of a liquid-based electrolyte to a fiber-based electrode results in something similar to a carbon-fiber reinforced plastic; carbon fibers surrounded by a polymer matrix. Based on this, the idea of a structural battery was born. By combining electrochemical and mechanical properties in the same material, a structural battery could function both as a structural element and as energy storage, having the possibility to become a fully integrated part of a device. In addition, an increase of power and energy density on a system level could be achieved. Portable electronics and HEVs are

some areas that would benefit greatly by the use of multifunctional materials in the form of structural batteries, especially since conventional batteries are considered to be purely structurally parasitic as they only add to the weight of the device and nothing to the structural integrity.

For a structural battery, both strength and stiffness are of great importance. The mechanical properties of the PAN-based carbon fibers make them very suitable for an application with these kinds of requirements. Commercially available carbon fibers will of course be more practical and cost-effective to use since it is relatively easy to obtain large volumes of high quality fibers produced in a reproducible way. In addition to the fibers, the surrounding matrix is also required to have sufficient mechanical properties, as well as ionic conductivity. Unfortunately, ionic conductivity and mechanical stability are conflicting properties in SPEs, related to the cross-linking density of the network. The best SPEs of today have shown conductivities as high as 10^{-5} S cm^{-1} [63], although standard liquid electrolytes have conductivities in the region of 10^{-2} S cm^{-1} [7]. But as a load-carrying component in a structural battery, a lower conductivity can be accepted due to the synergetic effect of multifunctionality. Previous studies have shown it possible, by using monomers with different functional groups, to tailor the properties of the polymer electrolyte so that adequate mechanical properties could be achieved while maintaining some of the conductivity[64-67]. Other advantages that can be achieved with SPEs are improved safety, temperature stability, and the possibility to fabricate batteries in any shape or size[68].

The design used for most of the "true" structural batteries, i.e. not the ones based on structural packaging[69,70], is based on a laminate structure similar to that used in conventional lithium-ion batteries, consisting of thin-film electrodes and solid electrolytes[71-74]. A laminar structured battery is relatively easy to manufacture but the drawback is the conductivity of the SPE. A solution to this problem is either to find better electrolytes or to decrease the transport distance of the lithium ions in the electrolyte.

Chapter 2

Scope of the Thesis

The aims of this thesis have been twofold and focused on the evaluation and characterization of existing battery technologies, and the development of electrodes for new concepts using electrochemical methods.

In recent years, $LiFePO_4$-based systems have become a popular choice since the chemistry is considered to be safe, inexpensive and environmentally benign[75]. The lifetime performance of $LiFePO_4$ has been investigated to develop an understanding of how this technology tolerates and is influenced by different conditions, such as cycling, storage and temperature. Since this project was partly funded by the Swedish automotive industry, the study was performed with focus on an automotive application. Cycle aging was, hence, investigated using a synthetic hybrid drive cycle. For this study a method was adopted which combined extensive electrochemical experiments with materials characterization and modeling for a thorough analysis of aging, and was performed in collaboration with other parties.

The second project has focused on the development of structural energy-storage composites i.e. structural batteries. Such batteries are desired for their possibility to reduce system weight and provide energy for future energy-storage applications, such as electric vehicles. To realize a structural battery, materials adapted for both electrochemical and mechanical usage must be developed for the negative and positive electrodes, as well as for the electrolyte and separator layers. Within this project, studies aimed at finding new suitable electrode and electrolyte materials, as well as how to design a structural battery, were initiated. However, the main part of the research included in this thesis has been focused on the different electrochemical and mechanical properties of commercially available carbon fibers as a structural negative electrode.

As a starting point for this study, the possibility to use commercially available PAN-based fibers as a multifunctional negative electrode was evaluated electrochemically. Since the microstructure of a carbon fiber is not only responsible for the intercalation but also the mechanical properties the impact of lithium intercalation on said properties is an equally important issue that needs to be addressed before carbon fibers can be deemed suitable for structural batteries. Therefore, experiments were performed to evaluate the effect of cycling on the tensile properties of carbon fibers.

Chapter 3

Experimental

3.1 Aging of $LiFePO_4$-based cells

The aging study was performed with laboratory-made pouch cells and based on mesocarbon microbeads (MCMB)/LiFePO4 graphite chemistry. The electrodes were supplied by Quallion LLC. Table 3.1 lists the cell specifications.

Table 3.1 *Cell specifications.*

Positive electrode	
Active material	$LiFePO_4$, Phostech P2 / 84 wt.%
Current collector material	Aluminum / 20 μm
Loading thickness	35 μm
Porosity	27 %
Loading density	8 mg cm^{-2}
Negative electrode	
Active material	MCMB graphite / 90 wt.%
Current collector material	Copper / 10 μm
Loading thickness	30 μm
Porosity	45 %
Loading density	3.8 mg cm^{-2}
Separator	
Material	PP/PE/PP, Celgard 2320
Thickness	20 μm
Porosity	39 %
Electrolyte	1M $LiPF_6$ EC:DEC (1:1 w/w), Merck LP40

The aging scenarios consisted of parallel cycle and calendar aging, performed at two different temperatures, 22 °C and 55 °C, and one state-of-charge (SOC), 60 %. A 300 seconds long charge-neutral synthetic hybrid drive cycle[76] with a 20 % SOC window, starting with discharge pulses from 60 % SOC (i.e. the cells were cycled between 60 % SOC and 40 % SOC) was used for the cycle aging (figure 3.1) while the calendar-aged cells were fixed potentiostatically at 60 % SOC.

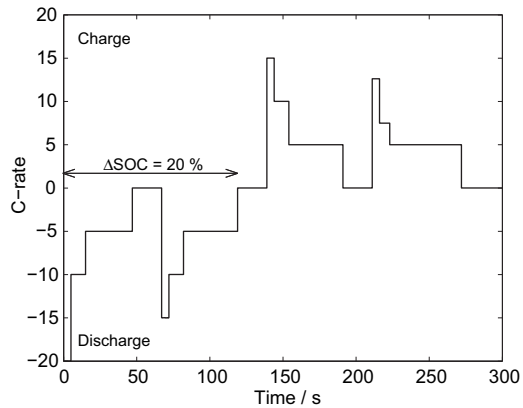

Figure 3.1 *Synthetic hybrid drive cycle used for cycle aging.*

To investigate the full cell performance degradation over time, reference performance tests (RPT) were conducted after every 500th cycle, at the target temperature. For the calendar-aged cells, the performance was tested at the same time as the cycled cells (**Paper I**). The RPTs included:

- 1C-discharge capacity evaluation based on beginning-of-life (BOL) nominal capacity.
- Potentiostatic electrochemical impedance spectroscopy (EIS) measured at 60 % SOC.

In addition to the RPTs, the resistance of the first discharge pulse of the hybrid cycle was used as a continuous, non-interruptive, reference performance test. The cells were continuously cycled until one of the two end-of-life (EOL) criteria was reached for the cycling cells. End-of-life was considered to have been reached when either less than 50 % of the nominal BOL 1C-discharge capacity remained or the synthetic hybrid drive cycle no

longer could be completed without reaching outside the cut-off voltages. The calendar aging was terminated when the cycle-aged cells reached EOL.

After reaching EOL, the cells were disassembled and the performance degradation of the harvested electrodes was investigated further combining electrochemical experiments with materials characterization and modeling for a thorough analysis of aging. The electrodes were evaluated electrochemically by capacity measurements (at 0.1C) and EIS in a three-electrode setup. SEM was used to examine the electrode morphology. The electrode/electrolyte interface composition, which is known to change during aging, was investigated using x-ray photoelectron spectroscopy (XPS) (**Paper I**). A physics-based EIS model, where the 0.1C-capacity measurements and SEM images served as input, was set up to analyze the experimental three-electrode EIS data (**Paper II,** cells aged at 22 °C). For comparison, the performance at BOL was also evaluated using the same approach. The methodology for detection of aging was, as for the full cells, based on the observable changes between BOL and EOL.

3.2 Carbon fibers

Working with carbon fibers in electrochemical applications requires special care since stray fibers easily cause short-circuits. Therefore, to facilitate handling, the fiber tows were equipped with tabs and attached to a non-shrinking heat-resistant paper, shown in figure 3.2, whenever experiments were performed on more than one fiber. Tabbing of the fiber tows enabled investigations of the effect of electrochemical cycling, i.e. lithium intercalation, on the mechanical properties both *ex situ* and *in situ*. Tensile tests were performed with a micro tensile stage, using fiber tows since single-fiber measurements are more sensitive to micro defects whereas a tow will have a predominantly ameliorative effect on the mean results. All electrochemical experiments were performed in laboratory-made pouch cells with carbon fibers as working electrode and lithium metal foil as counter electrode.

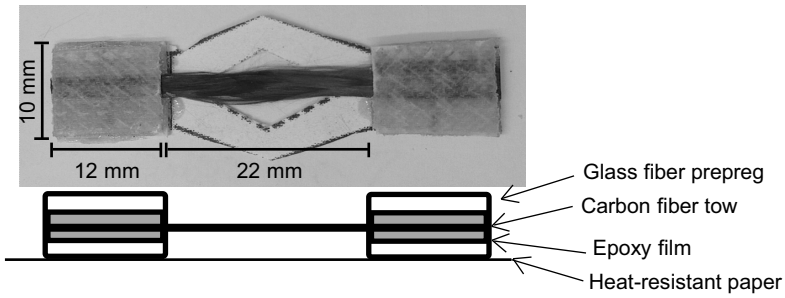

Figure 3.2 *Tabbed carbon-fiber specimen used for electrochemical and tensile testing.*

Commercially available carbon fibers are usually equipped with a coating, also known as sizing, consisting of either epoxy or polyurethane (PU) based resin to ease the handling and enhance the bonding between the fibers and the surrounding matrix in composite manufacturing. To distinguish between the different types of fibers, "desized" refers to a fiber where the sizing has been removed by washing in acetone and "unsized" refers to a fiber which has been taken out of production by the manufacturer prior to the sizing step.

3.2.1 Electrochemical characterization of commercially available fibers

Fiber tows – Several grades of fiber tow (table 3.2), with suitable mechanical properties, were chosen and evaluated electrochemically. The performance of the fibers was characterized in terms of specific capacity obtained after ten full cycles. The impact of sizing and lithiation rate on capacity were also investigated (**Paper III**).

Table 3.2 *Carbon fiber properties as specified by the manufacturers.*

Grade	Diameter /μm	Strength /MPa	Modulus /GPa	Sizing	Electrical Resistivity /Ωcm ×10³
T300	7	3530	230	Epoxy	1.5
T800	5	5490	294	Epoxy	1.4
M40	5	4410	377	Epoxy	0.8
M46	5	4210	436	Epoxy	0.9
UTS50	7	4800	240	PU	1.6
IMS65	5	6000	290	Epoxy	1.45
UMS45	4.7	4500	430	PU	0.97

Single fibers – To characterize the electrochemical properties of the carbon fibers further, an experimental investigation was performed on single IMS65 fibers. For this purpose a special pouch-cell configuration was developed to facilitate interpretation of the electrochemical measurements for modeling purposes. The cell was designed so that the negative current collector was encompassed in the heat seal of the pouch cell (figure 3.3) to avoid interference from the current collector on the measurements, i.e. only the carbon fiber was in contact with the electrolyte. An oversized lithium metal foil was used in order to also minimize any impact from the counter electrode on the measurements. The electrochemical properties, kinetics and mass transport, were mainly characterized using impedance spectroscopy and analyzed with a physics-based EIS model. The impedance measurements were performed for several SOCs (5-100 %) to investigate its effect on the properties for both unsized and sized fibers. In addition, the impact of SOC on the electronic conductivity was also studied. For comparison to the fiber tows the impact of sizing and lithiation rate on the capacity of single fibers were also investigated (**Paper IV**).

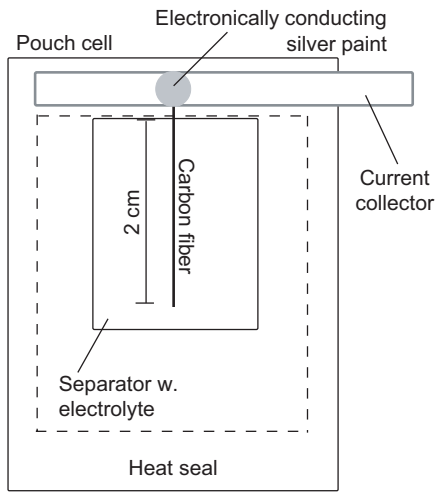

Figure 3.3 *Schematics of cell used for electrochemical measurements of a single fiber (counter electrode not shown).*

3.2.2 Impact of lithium intercalation on carbon fiber properties

The impact of lithium intercalation was investigated for two fiber grades, IMS65 and T800, in two different ways. The first way was to cycle fiber tows for an extended period of time and test the tensile properties *ex situ* after a certain number of cycles (1, 10, 100 and 1000) had been completed. Tensile properties were measured for cycled fibers in either lithiated or delithiated state and compared to uncycled fibers to determine the impact of intercalation (**Paper V**). The second way was performed *in situ* by applying a constant tensile extension to the pouch cell during cycling and measuring the variations of tensile load carried by the fiber tow, i.e. expansion in the longitudinal direction. The setup used for the second method is shown in figure 3.4. In addition, the transverse (radial) expansion was also investigated using SEM images of fiber cross-sections (**Paper VI**).

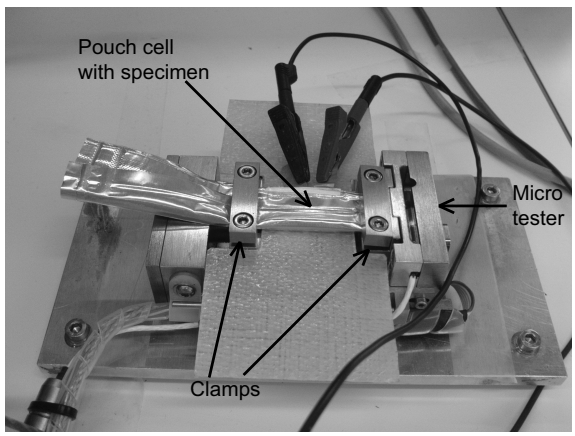

Figure 3.4 *Test setup for in-situ measurement of fiber expansion in the longitudinal direction.*

Chapter 4

Results and discussion

4.1 Observed effects of aging in $LiFePO_4$-based cells

Aging was investigated in laboratory-made pouch cells based on mesocarbon microbeads (MCMB) graphite/$LiFePO_4$ chemistry. Several methods, electrochemical, materials characterization and modeling, were used to evaluate the effect of aging. This section has therefore been divided into subsections accordingly, concluding with an overall discussion of performance degradation.

4.1.1 Full cell performance

At 22 °C, the cycled cells reached EOL after 14000 cycles (115 days including RPTs) while the cells cycled at 55 °C only managed 3000 cycles (25 days including RPTs) before reaching EOL. Total cycle lifetime at 22 °C was thus almost five times longer than at 55 °C. The development of the 1C-discharge capacity for the different temperatures and aging conditions over time is shown in figure 4.1. At 55 °C, the calendar- and cycle-aged cells showed a similar capacity-loss behavior. For the lower temperature, a more significant variation in capacity was observed between the calendar- and cycle-aged cells. At ambient temperature, cycling-induced processes appear to dominate the capacity loss while the contribution from cycling-related processes appears to be much less pronounced at 55 °C.

EOL was, as described in section 3.1, defined as either 50 % of the initial capacity or the inability to complete the synthetic hybrid drive cycle. At both 22 °C and 55 °C, cells failed due to the second criterion, the inability to sustain the high rates in the hybrid drive cycle within the specified voltage window.

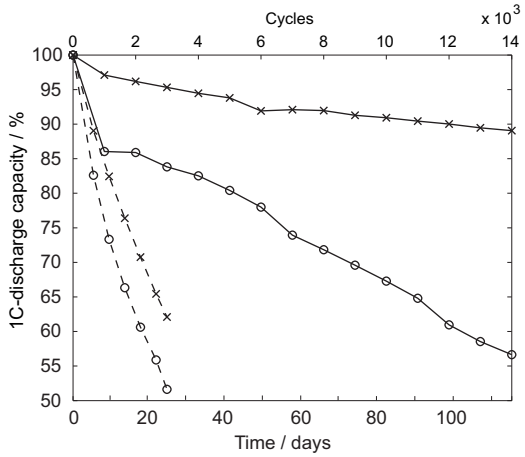

Figure 4.1 *Capacity retention compared to BOL over time for cycle and calendar-aged cells at 22 °C and 55 °C. Notations: cycle aged (o), calendar aged (x), 22 °C (solid lines) and 55 °C (dashed lines).*

The impedance measured for the 22 °C cycle-aged cell showed a slight change in the high-frequency semi-circle shape but with a similar magnitude and position of the curves compared to BOL (figure 4.2a). The impedance of the 22 °C calendar-aged cells was very similar to BOL, which indicated that no major performance degradation had occurred. This is also supported by the 1C-capacity retention in figure 4.1. At 55 °C, the impedance of the cycle-aged cells displayed variations at both high and low frequencies, showing an increased number of semi-circles and changes in the slopes of the low-frequency tails, respectively. The 55 °C calendar-aged spectrum, unlike its ambient temperature counterpart, displayed similarities to the 55 °C cycle-aged cells (figure 4.2b). The different results seen at low frequencies for cells cycled at the two temperatures might be interpreted as differences in mass transport in the active electrode material and electrolyte, whereas the increased number of semi-circles at higher frequencies can be interpreted as resistance changes in different parts of the cell.

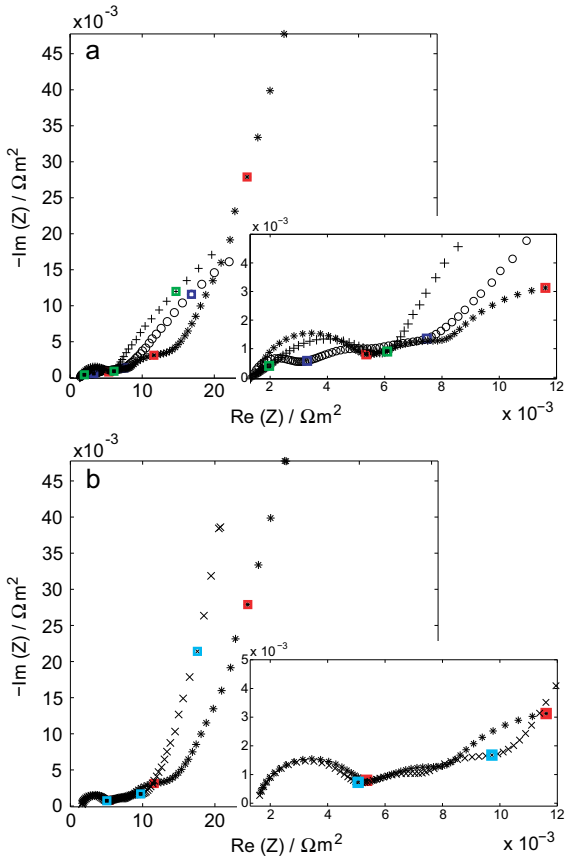

Figure 4.2 *Full cell EIS measured at a) BOL (+) and EOL for cycle-aged cells at 22 °C (o), and 55 °C (*), and b) 55 °C cycle (*) and calendar-aged cells (x). Inset: Magnification of the high-frequency area. Colored squares (□) denote frequencies 1000, 1 and 0.01 Hz for the different cells.*

In this study, only two different interruptive RPTs were used during the lifetime in order to maximize the cycle time and minimize aging caused by the RPTs themselves. It was therefore advantageous to use the existing data from the synthetic hybrid drive cycle as an additional performance test. So by using the data from the initial five second 20C-discharge step, any variations in discharge resistance over time could be monitored. A current pulse resistance, like the one described above, can be divided into two different contributions[77]:

- The instantaneous voltage drop related to contact resistances, activation polarization and ohmic potential drop in the electrolyte, i.e. ohmic losses.

- The voltage changes during the pulse, related to diffusion polarization in the electrolyte and active electrode material.

The discharge resistances were also used to gain further insight into the impedance changes during cycle aging, and can be considered as complementary in the sense that they demonstrate the resistance evolution at the target temperatures, 22 °C and 55 °C, while the impedance spectra were acquired at room temperature for the cycle-aged cells.

The total increase of the discharge resistance was most pronounced at 55 °C, and dominated by ohmic losses (figure 4.3b). At 22 °C, the time-independent ohmic losses and time-dependent diffusion polarization showed more equal contributions to the total discharge resistance over time (figure 4.3a). However, it is important to consider the effect of the different measurement temperatures between the two methods when comparing the results. If the discharge-resistance measurements had been performed at ambient temperature the losses caused by cycling at 55 °C would have been even more substantial, as the impedance measurements showed. Interestingly, for both temperatures the current pulse resistance data showed, like the impedance, that the diffusion polarization increases during prolonged cycling, indicating changes in the pore structure of the electrodes. Changes in pore structure of the electrode and separator will also affect the effective conductivity and may thus influence the time-independent losses to some extent as well.

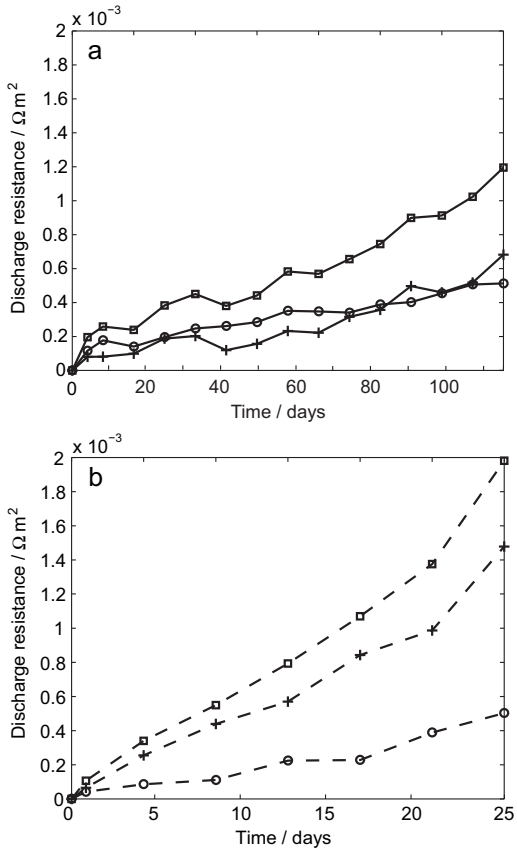

Figure 4.3 *Discharge resistances relative to BOL for cells cycle aged at a) 22 °C and b) 55 °C. Notations: total resistance (□), time-independent ohmic losses (+), and diffusion polarization in the electrolyte and active material (o).*

4.1.2 Materials characterization results

After reaching EOL, the cells were disassembled and the electrodes were harvested for materials characterization, using SEM and XPS.

Cycle-aged negative electrodes – At BOL (figure 4.4a), an electrode with a clear porous structure composed of MCMB graphite particles of different sizes and shapes was observed using SEM. After aging at 22 °C, the SEM showed an electrode with smoothened contours due to surface cracking (inset figure 4.4b), and a reduced porosity compared to BOL. After aging at 55 °C, the electrode

displayed a substantial decrease in porosity with a thick surface layer of electrolyte decomposition products (figure 4.4c).

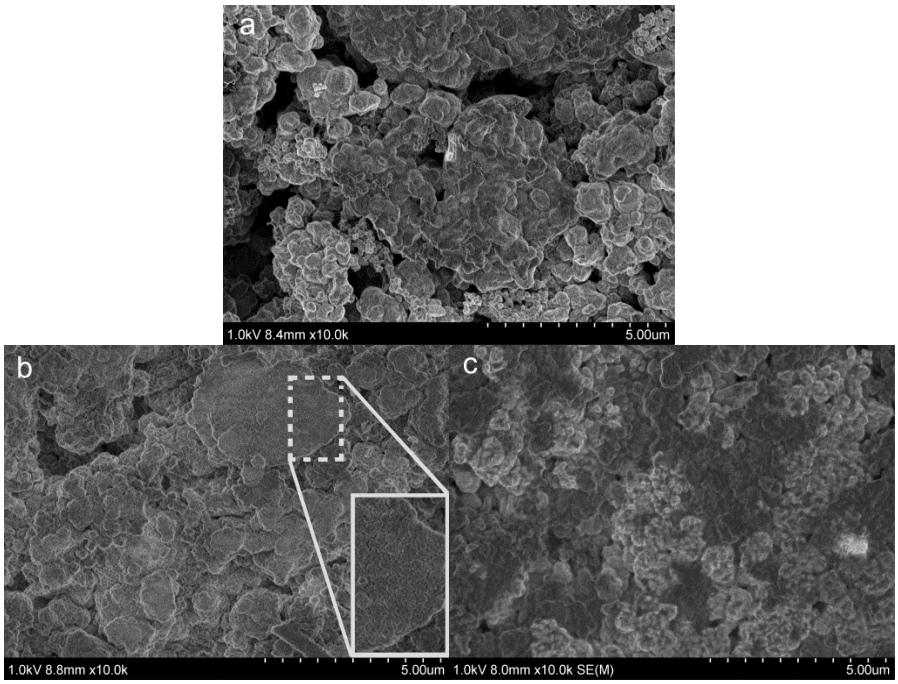

Figure 4.4 *SEM images of harvested negative electrodes (a) at BOL, and after cycle aging at (b) 22 °C and c) 55 °C.*

From the XPS, some interesting differences were detected between the electrodes cycle-aged at the two temperatures. At 55 °C, larger relative amounts of LiF and P-O containing compounds were detected than at 22 °C. Cycling at elevated temperatures is, however, known to cause an accelerated decomposition of the $LiPF_6$ salt[78], which would explain the differences observed by XPS and SEM. Elevated temperatures have also been reported to affect decomposition products towards more stable but less ionically conductive inorganic products[79,80]. For both temperatures, the XPS results showed that the relative amounts of deposited electrolyte products were so large that the signal from the MCMB graphite was no longer visible. This indicates that increased amounts of electrolyte products had become deposited on the electrode surfaces during cycle aging. However, due to the limited probing depth of the XPS instrument used in this study it was not possible to determine the thickness of the deposited electrolyte products at the two

temperatures. In general, elevated temperatures are considered very detrimental to the stability of the negative electrode SEI and often regarded as the main reason for cell aging under such conditions[9].

Cycle-aged positive electrodes – The electrode morphology at BOL (figure 4.5a) displayed a clear porous structure just as for the negative electrode, but with a lower porosity due to the smaller $LiFePO_4$ particles, which is in accordance with the electrode specifications in table 3.1. From the SEM images, the morphology of the 22 °C electrode (figure 4.5b) appeared significantly altered compared to BOL with deposits partly covering the surfaces, cracks in the active material particles at several locations (circled areas in figure 4.5b), and a decreased porosity. At 55 °C (figure 4.5c), the overall morphology seemed less affected by aging and more similar to BOL than at 22 °C.

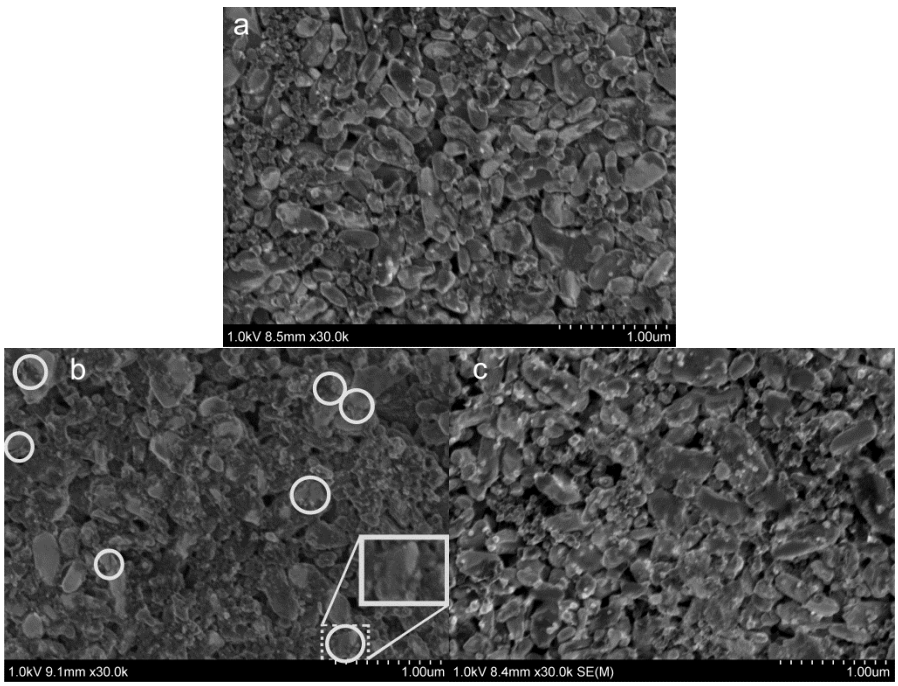

Figure 4.5 *SEM images of harvested positive electrodes (a) at BOL, and after cycle aging at (b) 22 °C and c) 55 °C.*

In several cases, the XPS of the positive electrode/electrolyte interfaces displayed similar trends in composition as the corresponding negative ones. The XPS results also indicated, similarly to the negative electrode, that the

relative amounts of deposited electrolyte products were so large that the signal from the phosphate in the $LiFePO_4$ was hardly visible. This seems to be somewhat contradictory to the indications from the SEM images where the 55 °C electrode exhibited less visible signs of aging than at 22 °C. However, if the layer of decomposition products on the electrode was thin enough this might not be visible with the SEM but with XPS, since the latter is a more surface-sensitive technique. An additional difference between the electrodes used for XPS and SEM is that the former was not washed prior to the measurement, which could also possibly explain the discrepancy.

Calendar-aged electrodes, 55 °C – The impact of cycling on the electrolyte degradation was investigated comparing XPS of 55 °C cycle- and calendar-aged electrodes. The XPS of the calendar-aged electrodes showed significant differences in electrode/electrolyte interface compositions compared to the cycle-aged case, indicating that cycling causes other electrolyte degradation processes than storage. The difference in electrolyte decomposition on cycling and storage aging has previously been suggested in the literature[19]. In contrast to the significant differences in XPS, both the capacity loss and the impedance increase of cycle- and calendar-aged cells at 55 °C were comparable. These results are most noteworthy and indicate that the cells, in spite of differences in the electrolyte decomposition processes, can exhibit similar appearance in electrochemical performance degradation.

4.1.3 Harvested electrode evaluation

In addition to the materials characterization, the harvested electrodes were also evaluated electrochemically and with a physics-based EIS model. For this purpose, the harvested electrodes were reassembled in a three-electrode setup, using new electrolyte and separator, and the 0.1C-discharge capacity and EIS at 60 % SOC were measured. At 22 °C, the capacity of the cycle-aged positive and negative electrodes had decreased by 15 % and 9 %, respectively. At 55 °C, however, no significant changes in capacity could be detected for the cycle-aged positive electrode, but the corresponding negative electrode had lost 12 % in capacity compared to BOL.

Cycle-aged negative electrode, 22 °C – The impedance spectrum showed a significant increase of the semicircle and a shift along the real axis (figure 4.6). From the EIS model analysis, a considerable increase in resistive surface films

and decrease in electrode porosity were detected compared to BOL. The resistive surface film and porosity decrease correspond to the XPS results where the contribution from the active material was no longer visible due to deposition of electrolyte products, as well as the results from SEM. The decomposition of the electrolyte is, in this case, most likely caused by exposure of fresh electrode material on the surface connected to the intercalation-induced volume changes. Exposed electrode material is also more susceptible to graphite exfoliation due to co-intercalation of solvent molecules which would account for the observed loss of active material (9 %).

Cycle-aged positive electrode, 22 °C – The three-electrode impedance measurement showed a substantial change compared to BOL; the semicircle has become expanded in both the imaginary and real directions and the minimum in imaginary impedance at the beginning of the low-frequency tail has disappeared (figure 4.6). The results from the EIS model analysis showed, as suggested from the SEM images, a substantial decrease in electrode porosity, particle cracking and loss of active electrode material. The observed active electrode material loss (15 %) was suggested to be caused by isolation of pieces of the porous electrode rather than by cracking of separate particles. The decrease in porosity is likely the result of deposition of electrolyte decomposition products since most of the surface was covered with deposits according to the XPS characterization. Even though similar effects of aging were observed on both the positive and the negative electrode, the impact on performance was different. A possible explanation for this is that the positive electrode has a lower porosity to begin with (27 %) compared to the negative electrode (45 %), making it more susceptible to deposition of electrolyte decomposition products.

Cycle-aged electrodes, 55 °C – Preliminary results from the EIS model analysis on the electrodes cycle-aged at 55 °C indicated that a substantial increase in resistive surface film growth and subsequent decrease in the negative electrode porosity had occurred. The positive electrode showed signs of increased contact resistances and a minor change in porosity.

4.1.4 Correlation of electrode aging on full cell performance

Aging at ambient temperature – At EOL, the full cells aged at 22 °C had lost 11 % (calendar) and 44 % (cycled) in 1C-discharge capacity**.** Due to the rate used for the capacity evaluation there is a need to separate the contributions of polarization due to impedance increase and available charge (cyclable lithium and active electrode material) on the measured data. The different contributions were deciphered using the harvested electrode EOL performance, as explained in detail in Paper II, section 5.3. In the calendar-aged case, the decrease in full cell 1C-discharge capacity was caused by loss of cyclable lithium. However, both loss of cyclable lithium (~84 %) and cell impedance increase (~16 %) were suggested as the source of capacity loss in the cycle-aged case. Loss of cyclable lithium is, as described above, most likely to originate on the negative MCMB graphite electrode. In this study only the degradation of the harvested electrodes could be detected since new electrolyte and separator were introduced in the three-electrode setup. Therefore, performance degradation related to the electrolyte and separator, such as decreased electrolyte wettability and changes in separator porosity, are not accounted for.

Even though both electrodes showed clear signs of aging, the positive electrode contributed more to the full cell performance degradation and impedance increase. This can be seen in figure 4.6 where the full cell, and positive and negative electrode impedance at BOL and after cycle aging at 22 °C is presented. At BOL, the full cell shows a strong resemblance to the positive electrode compared to the negative electrode. This resemblance also remains at EOL, showing that the positive electrode is limiting at ambient temperature. The overall cause of performance degradation after cycle aging at 22 °C is capacity fade due to loss of cyclable lithium from electrolyte decomposition reactions. However, deposition of the electrolyte decomposition products also resulted in increased impedance due to the buildup of resistive surface films on the negative electrode, and a decreased porosity in both electrodes.

Aging at elevated temperature – For 55 °C, where the assumption that most of the loss of cyclable lithium occurs electrochemically might not be correct, deciphering the contributions to the 1C-discharge capacity is not as straightforward. However, the data in figures 4.2 and 4.3 and the XPS results

indicate that a larger part of the 1C-discharge capacity loss (figure 4.1) in the cycle-aged case originates from an impedance increase due to the substantial changes in mass transport and discharge resistance compared to at 22 °C. The preliminary results also indicate that the negative electrode seems to limit the lifetime at elevated temperature, while the positive electrode was shown to be limiting at ambient temperature.

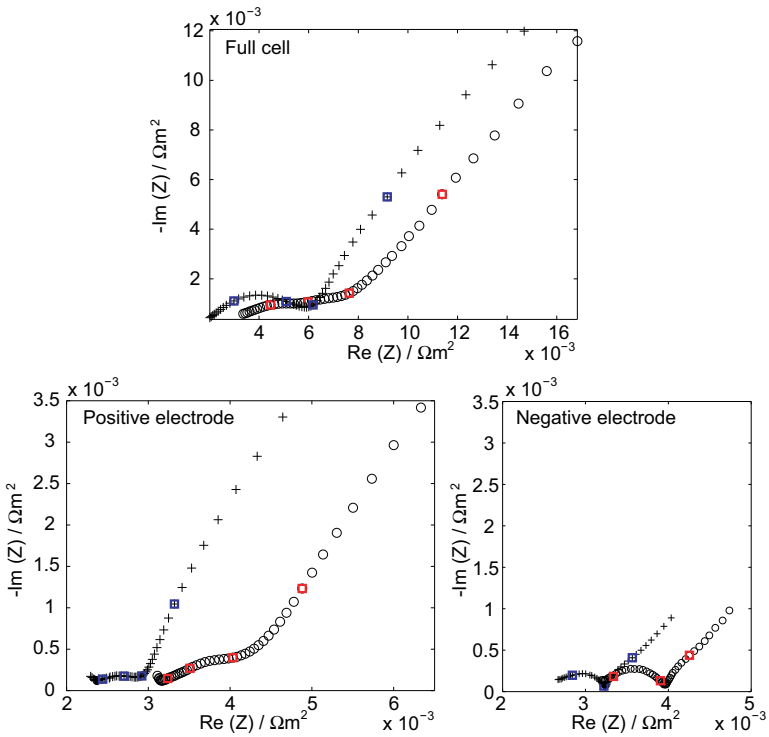

Figure 4.6 *Full cell and harvested electrode EIS spectra (1000 Hz – 10 mHz). Notations: BOL (+) and 22 °C cycle aged (o). Blue and red squares (□) denote frequencies 100, 10, 1 and 0.05 Hz for BOL and EOL, respectively.*

4.1.5 Overall discussion of performance degradation

The XPS, SEM and modeling results obtained from the harvested electrodes all indicated that layers of electrolyte decomposition products had become deposited in the pores of the electrodes. Deposition of electrolyte decomposition products causes the electrode porosity to decrease, which impairs the mass transport, but also results in the formation of resistive surface

films, which increases the ohmic losses. Electrolyte decomposition also consumes lithium ions which results in capacity fade and imbalance between the electrodes, as illustrated in figure 1.2. The observed changes in electrode performance and morphology can effectively account for the performance degradation of the full cells. However, depending on aging temperature, the cause for impedance increase varied. At ambient temperature the positive electrode was shown to be limiting while the negative electrode seemed to limit the lifetime at elevated temperature.

An important thing to remember about the system investigated in this thesis is that the electrolyte did not contain any additives. Commercial cells, however, usually include a cocktail of different additives to improve the cyclability and lifetime of the cells, as well as their safety[81]. Improved performance can be achieved with additives that 1) facilitate the formation of SEI on graphite, 2) reduce the irreversible capacity of the SEI formation and extended cycling, 3) enhance thermal stability of $LiPF_6$ against the organic electrolyte solvents, 4) protect positive material from dissolution (mainly manganese-based materials) and overcharge, and 5) improve electrolyte properties such as ionic conductivity, viscosity, wettability of the polyolefin separator. Several of the above listed additive properties could have improved the lifetime significantly, if added to the investigated system.

The finding that different electrolyte decomposition processes can result in similar appearance in electrochemical performance degradation implies the necessity to combine electrochemical methods with other techniques to investigate aging. The cells which were cycle-aged at the two temperatures also showed different electrochemical performance, as well as XPS results, at EOL. These results all confirm that aging is a complex set of processes which becomes accelerated to different extents at different temperatures. This raises the question of whether elevated temperatures can be used as a representative scenario for accelerating aging to investigate performance degradation at ambient temperature. Elevated temperatures should therefore be used with care for anything other than a "worst-case scenario" investigation.

4.2 Carbon fibers

In this section, the possibility of using commercially available PAN-based fibers as multifunctional negative electrodes is evaluated and discussed from electrochemical and mechanical points of view.

4.2.1 Electrochemical performance of fiber tows

All of the tested fibers showed some ability to intercalate lithium ions. However, the reversible capacity of the fiber tows varied significantly between the different grades when cycled at 100 mA per gram of fiber, ranging from 177 mAh g^{-1} for unsized IMS65 to only 24 mAh g^{-1} for desized UTS50 after ten full cycles. The capacity retention over ten cycles for a selection of fibers can be seen in figure 4.7. Of all the tested fibers IMS65, T800 and T300 were found to be the most promising ones, regarding capacity. The results also indicated that fibers with intermediate modulus (T800 and IMS65) have better electrochemical properties than those with high modulus (UMS45). Tensile modulus is a property not only related to the degree of graphitization but also to the alignment of the graphitic basal planes in the fiber[56], factors that will have a distinct effect on the ability to intercalate lithium ions.

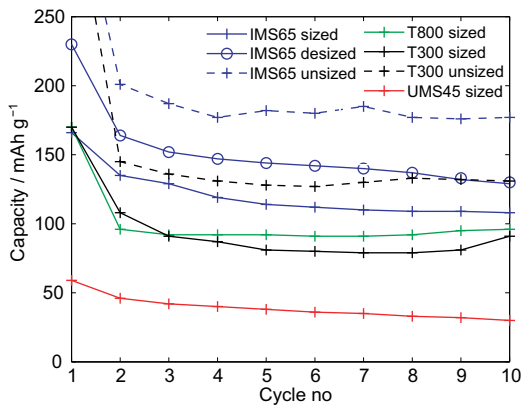

Figure 4.7 *Capacity retention over ten cycles for a selection of the tested fiber tows.*

Impact of sizing and rate on capacity – Comparing the obtained results for the sized, desized and the unsized samples of the IMS65 fiber (figure 4.7), it is evident that the sizing has a large influence on the reversible capacity for this specific fiber. Similar results were observed for sized and unsized T300, where the

latter had a capacity of 130 mAh g^{-1} compared to less than 100 mAh g^{-1} for the former. For some of the other fibers (T800 and UMS45) the impact of sizing was less pronounced.

The capacity was found to be very dependent on the lithiation rate, as shown in figure 4.8 for a tow of unsized IMS65; a reduction in current by a tenth resulted in a twofold increase in capacity. This trend was also observed for sized T800 and sized IMS65 fibers.

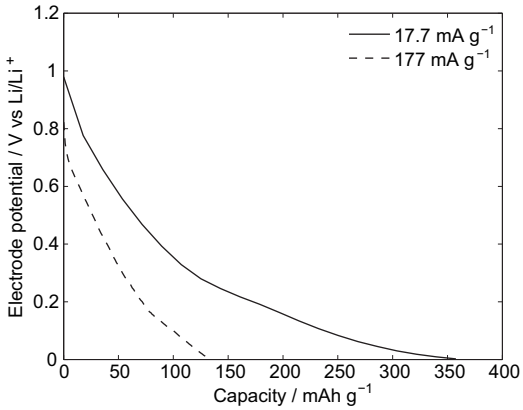

Figure 4.8 *Capacity of an unsized IMS65 fiber tow for two different lithiation rates.*

4.2.2 Electrochemical properties of single fibers

In order to fully determine the utility of carbon fibers as electrode material, the intrinsic electrochemical properties needed to be investigated. To investigate these properties, single fibers were used together with other well-characterized battery components. The properties were mainly determined from EIS measurements by fitting of a physics-based model.

From the experimental EIS data alone, a strong dependence on SOC could be distinguished for both the unsized and sized fibers. Both the charge-transfer resistance and mass transport, described by the exchange current density and solid-phase diffusion coefficient, respectively, appeared to improve with higher SOC. Like the impedance, the electronic conductivity also seemed to depend and improve with SOC. However, no distinct influence of sizing could be observed from the EIS measurements.

The results from the EIS model analysis affirmed the experimental observations that both the mass transport and exchange current density improves with higher SOC. This SOC dependence clearly indicates that the fiber microstructure becomes more favorable with lithium intercalation. The optimized diffusion coefficients and exchange current densities for unsized and sized IMS65 at 5-100 % SOC are shown in figure 4.9a and b, respectively. From the optimized parameters, just like the experimental data, it was not possible to distinguish any differences in electrochemical performance with sizing. Thus, sizing seems to have an impact only on tow level and should therefore be considered a tow property.

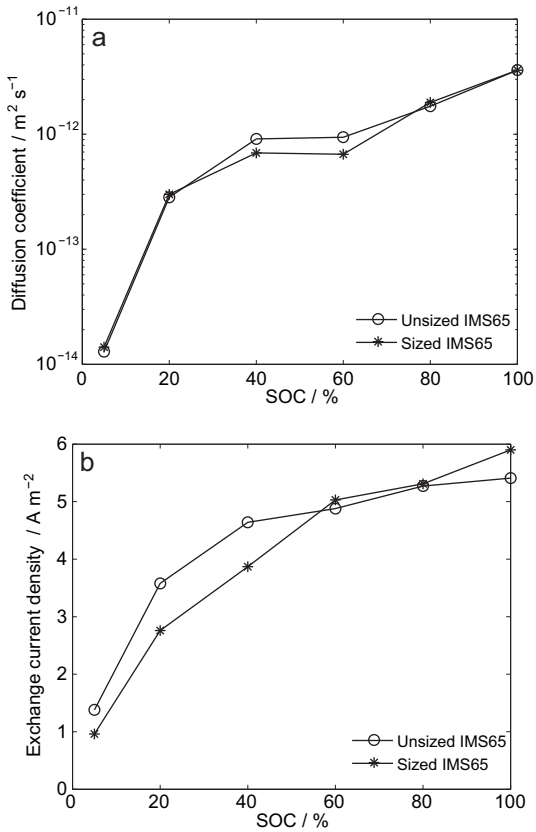

Figure 4.9 *Optimized a) diffusion coefficients and b) exchange current densities for single unsized and sized IMS65 fibers.*

In figure 4.10 the performance of a single unsized IMS65 fiber, lithiated at two different rates, is shown. At slow rates, the performance is very similar to that observed for a tow of unsized IMS65 (figure 4.8). However, at faster rates the tow exhibits a much lower capacity than the single fiber. The cause for the deviation is that a tow, unlike a single fiber, shows similarity to a porous electrode, though a very poor one, which increases the polarization of the cell at higher currents. This observation is also in agreement with the finding that to fit an electrochemical model to experimental EIS data, from a tow-based cell, an advanced porous geometry was required to describe the electrode.

One of the functions of sizing is to keep the fibers in a tow together to ease handling. A tow with the sizing intact will, therefore, most likely have a different porous structure than one where the sizing has been removed. The varying impact of sizing seen on the capacity of tow-based cells could, hence, be explained by differing porous structures in the presence or absence of sizing. Sizing can possibly also affect the electrolyte wettability of the fibers so that only parts of the tow are in contact with the electrolyte and therefore the capacity is negatively affected at higher rates.

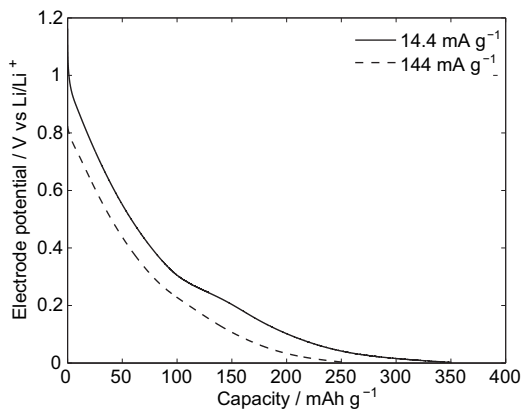

Figure 4.10 *Capacity of a single unsized IMS65 fiber for two different lithiation rates.*

Compared to other carbon materials investigated using the same method[43,82], single IMS65 fibers displayed excellent kinetic and mass transport properties, especially at high SOCs. Hence, in a battery application, separated fibers will be much more beneficial than tows for maximizing the utilization of the material.

4.2.3 Impact of lithium intercalation on the mechanical properties of carbon fibers

Ex-situ evaluation – The impact of lithium intercalation on the mechanical properties, the ultimate tensile strength and the tensile stiffness, was investigated. Ultimate tensile strength corresponds to the maximum tensile stress (force) a material can withstand before failure, while the tensile stiffness is measured as the slope of a tensile curve (force (N) vs. extension (%)) where the deformation is linearly elastic.

Figure 4.11 presents normalized tensile test curves of IMS65. The tensile stiffness appears to be unaffected by lithium intercalation and cycling since the slopes of all curves remain unchanged. The ultimate tensile strength, however, shows a distinct variation with SOC. After lithiation, the ultimate tensile strength of the fiber drops and is partly recovered when the fiber is delithiated again. The magnitude of the drops in strength remained reversible and unchanged for more than 100 cycles. After 1000 cycles, the capacity of the cell had decreased considerably and therefore the loss in tensile strength was reduced as less lithium was intercalated into the fibers. Cell failure was attributed to the degradation of the lithium counter electrode. In addition to the reversible drops in ultimate tensile strength, an initial irreversible loss occurred after the first lithiation. A permanent loss in strength suggests that some lithium becomes irreversibly intercalated in the fiber.

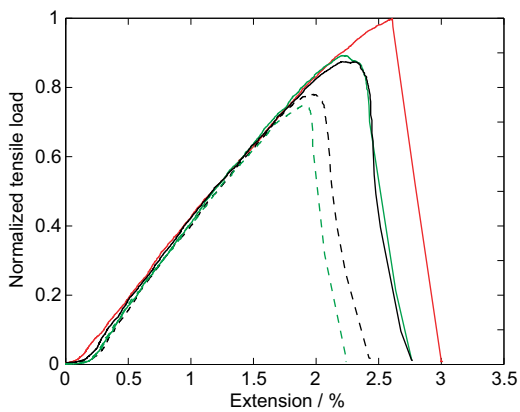

Figure 4.11 *Tensile curves of desized IMS65 fiber tows. Notations: Uncycled (red), after 10 cycles (green) and 100 cycles (black) at lithiated (dashed line) and delithiated (solid line) states.*

The trends of the changes in the tensile properties were similar for both grades of fiber. Even though the fibers exhibited some changes in tensile strength with SOC the magnitude was low enough to not compromise the applicability of the carbon fiber as structural electrode.

4.2.4 Intercalation-induced expansion

As observed from the *ex-situ* evaluation, the ultimate tensile strength of the carbon fiber drops upon lithium intercalation and the magnitude of the drop seems to be connected to the amount of intercalated lithium. Since intercalation of lithium ions is known to cause volume changes in carbons, both longitudinal and transverse expansions of the fiber are expected to occur as a result. For example, in graphite, the interlayer spacing increases by about 10 %, with a simultaneous expansion of about 1 % of the basal planes as lithium ions are intercalated[51,52,83,84].

Longitudinal expansion – In figure 4.12 the variations in tensile load carried by IMS65 specimens subjected to constant extension during electrochemical cycling at several rates are shown. As a reference, to distinguish the variations of the load carried by the specimens, a separate test measuring the load relaxation of the bag was performed.

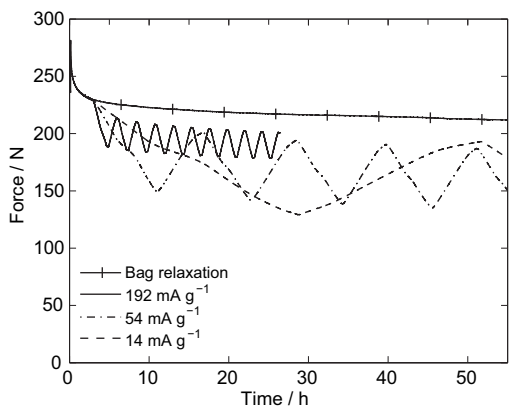

Figure 4.12 *Lithium intercalation induced expansion of IMS65 at different rates. Notations: Bag relaxation (+), 192 mA g^{-1} (solid line), 54 mA g^{-1} (dash dotted line), and 14 mA g^{-1} (dashed line).*

During lithiation, the fiber expands and the force drops with a reversal of the effect during delithiation, which causes the load to fluctuate upon cycling. Both the frequency and amplitude of the fluctuations vary with cycling rate. However, the variations in amplitude are caused by the mass-transport limitations arising in the fiber tow with higher cycling rates, as described above. For a fully lithiated fiber, with a capacity approaching 372 mAh g^{-1}, the reversible longitudinal expansion is approximately 1 %. This is especially noteworthy, as the basal planes in the microstructure of a carbon fiber tend to be oriented more parallel to the longitudinal axis[56,85]. The longitudinal expansion is of the same magnitude as for graphite which suggests that it is caused by a volume change in the basal planes. This longitudinal expansion might correspond to an internal tensile stress in the carbon fiber, which is also supported by the changes in ultimate tensile strength observed from the *ex-situ* study.

Like the *ex-situ* experiments, a permanent expansion was observed after the first lithiation, for all rates. For the subsequent cycles, however, the expansion was reversible. Hence, the irreversible intercalation of lithium ions occurs during the first cycle and must therefore contribute to the initial irreversible capacity loss of the cell together with the SEI formation. Since the capacity corresponding to the SEI formation is unknown, the amount of trapped lithium cannot be calculated directly from the first cycle. However, the capacity dedicated to the irreversibly intercalated lithium ions can be estimated assuming that 1) for the following lithiations no more SEI is formed and the capacity originates from intercalation only, and 2) the ratio of any capacity dedicated to intercalation and induced expansion remains constant for all cycles, as explained in detail in Paper VI, section 3.4.

The estimation of the capacity that corresponds to trapped lithium is shown in figure 4.13, together with the reversible capacity and the initial irreversible capacity loss, for five cycling rates. At lower rates, the initial irreversible capacity loss displays a stable behavior but decreases as the rates increases. However, at the lower rates, more and more lithium becomes irreversibly intercalated (trapped) in the fiber. The difference between the irreversible capacity and the trapped lithium is attributed to the SEI formation, which seems to vary with rate and exhibits a maximum for intermediate rates. These results suggest that a larger part of the initial capacity loss originates from

irreversible lithium intercalation, and less from SEI formation, at the highest and the lowest rates.

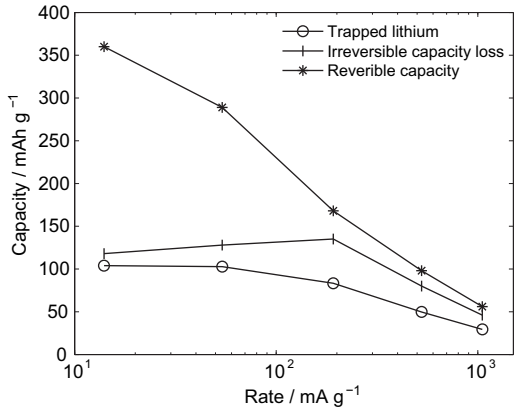

Figure 4.13 *Irreversible capacity loss, trapped lithium, and reversible capacity at different cycling rates for IMS65.*

Transverse expansion – The SEM investigation of cross-section areas revealed a transverse expansion between 8 % and 13 % for a fully lithiated fiber, and 2-3 % for a delithiated fiber, indicating that an expansion also occurs in the radial direction of the fiber upon lithium intercalation. Like the longitudinal expansion of the carbon fiber, the transverse expansion correlates to the increase in interlayer spacing upon intercalation seen in graphite. However, due to the disordered microstructure of the studied carbon fibers, some differences might be expected compared to the crystalline graphite. Nevertheless, as the results suggest, the expansion caused by lithium intercalation is governed by the expansion between and in the graphitic basal planes. Similar expansions were observed for both fiber grades, and since both display comparable mechanical properties their microstructure must have some kind of resemblance. For an application such as a structural battery, where the mechanical properties are of paramount importance, expansions like these need to be taken into consideration in the development process.

4.2.5 Overall discussion of carbon fibers

The electrochemical evaluation of commercially available PAN-based carbon-fiber tows showed that all of the tested grades displayed some ability to

intercalate lithium ions. As tows, the fibers would not be suitable for any application which requires high current loads other than one where the mechanical properties are also needed. However, further studies revealed that single fibers have superior electrochemical properties compared to other negative electrode materials. Single or properly separated fibers could, in addition to structural-battery applications, possibly replace the powder-based negative electrodes commonly used in lithium-ion batteries. However, an issue that inhibits the usage of carbon fibers in conventional battery applications is the cost. According to the manufacturers, the cost of carbon fibers range between 3 and 30 times that of battery-grade graphite powders, depending on the grade of fibers. Carbon-fiber electrodes would also require a new manufacturing process for the batteries, but with the benefit of excluding the binder and therefore a lot of solvent, and reducing the amount of copper current collector. In all, carbon-fiber electrodes could contribute to the reduction of weight in conventional lithium-ion batteries as well.

For carbon fibers to be used in structural batteries, however, some issues need to be addressed specifically, such as the drawbacks of fiber tows and the intercalation-induced volume changes, to achieve optimal energy storage and structural performance in a final application.

In order to realize a structural battery, extensive research into electrolyte systems and positive electrodes with suitable electrochemical and mechanical properties will be required. However, due to the required multifunctionality of these materials, this will be a very challenging task.

Carbon fibers could, in addition to pure battery applications, also be used for actuation or sensor applications. These other application areas would utilize the intercalation-induced reversible longitudinal expansion of the fiber to provide mechanical work as operating mechanism.

Chapter 5

Conclusions

The aim of this thesis has been to evaluate and characterize the performance of two different lithium-ion battery systems. Similar techniques were used for the investigations, extensive electrochemical experiments with materials characterization and modeling. This proved to be a very powerful toolbox.

5.1 Aging in $LiFePO_4$-based cells

The lifetime performance of the MCMB graphite/$LiFePO_4$ system was investigated to develop an understanding of how this technology tolerates and is influenced by different conditions, such as cycling, storage and temperature. Overall, elevated temperature was, unsurprisingly, found to be the most detrimental condition to the lifetime of the tested system. Cycling at elevated temperature resulted in a significantly reduced lifetime, almost five times shorter compared to cells cycled at ambient temperature. Calendar lifetime was also considerably reduced at elevated temperature. For the cycling cells, the cause of EOL was, independently of temperature, the inability to complete the synthetic hybrid drive cycle. Both full cell impedance and discharge-resistance measurements indicated an increase in ohmic losses and diffusion polarizations for the cycle-aged cells.

The negative and positive electrodes, harvested from the cycle-aged cells, displayed extensive deposition of electrolyte decomposition products at both temperatures. This was found to be the main cause of aging in the full cells as it consumes cyclable lithium, i.e. capacity fade, and changes the morphology of the electrodes which increases the impedance. However, the target temperature at which the cycling was performed seemed to affect which electrode dominated the impedance increase. At ambient temperature, the positive

electrode was the limiting one, and at elevated temperature, the negative electrode showed more substantial signs of aging.

From the XPS on cycle and calendar-aged electrodes at 55 °C some interesting dissimilarities in electrolyte decomposition were found. In contrast to the significant differences in XPS, both the full-cell capacity loss and impedance increase of cycle- and calendar-aged cells at 55 °C were comparable. These results indicate that the cells, in spite of differences in the electrolyte decomposition processes, can exhibit similar electrochemical performance degradation, i.e. lithium-ion battery aging is a complex set of processes which becomes accelerated to different extents at different temperatures. These findings also imply the necessity of combining electrochemical methods with other characterization techniques to investigate all aspects of aging.

5.2 Carbon fibers

As a starting point for the development of structural batteries, the possibility of using commercially available PAN-based fibers as a multifunctional negative electrode was evaluated both electrochemically and mechanically.

The electrochemical performance of single carbon fibers was found to be excellent compared to other negative electrode materials. A strong SOC dependence was seen in the mass transport and kinetic (exchange current density) properties, as well as electronic conductivity, which all improved with lithiation. Sizing was established to have no impact on the electrochemical properties of single fibers and should only be considered a tow property.

The mechanical properties, measured as changes in the tensile properties of carbon-fiber tows, showed that the tensile stiffness was unaffected by lithium intercalation and cycling. The ultimate tensile strength, however, showed a distinct variation with SOC. Similar to graphite, the carbon fibers demonstrated a reversible longitudinal and transverse expansion induced by lithium intercalation, correlating to an increase in the interlayer spacing by about 10 %, and a simultaneous expansion of about 1 % of the basal planes, at 100 % SOC. In addition to the reversible expansion, an irreversible expansion occurred after the first lithiation. This was attributed to the irreversible intercalation of lithium ions and was found to depend on the rate of intercalation during the first lithiation.

Overall, carbon fibers can be considered suitable for structural batteries; however, some issues need to be addressed specifically, such as the drawbacks of fiber tows and the intercalation-induced volume changes, to achieve optimal energy storage and structural performance in a final application.

6 Acknowledgments

First of all I would like to thank my supervisor Göran Lindbergh for giving me this opportunity to work on these very interesting and challenging research projects. Mårten Behm is also gratefully acknowledged for the co-supervision and assistance in the more practical parts of my research.

Special thanks to my fellow PhD students in the battery group for all the laughs and crazy (sometimes inappropriate) YouTube-Nåndag videos.

Thanks to Matilda, Pontus and Tommy for valuable and smooth collaborations in the field of batteries.

To all former and present colleagues at TEK; without you these years would not have been as enjoyable.

I would also like to thank everybody in the KOMBATT project for the interesting discussions and productive collaborations on structural batteries, and for all the memorable project meetings, especially the one with the volcanic eruption, ice fishing and snowmobiles.

My collaborators in the Gröna Bilen 2 and FFI projects, especially Sara Malmgren and Kristina Edström at the Ångström Laboratory, Uppsala University, are gratefully acknowledged.

Simon: 14 years in school together so far…. It started with the building of bridges, where will it end?

Finally, I would like to express my gratitude to my family: Mom, Roger and Tobias, for always supporting and encouraging me in everything I do.

7 References

1. U.S. Department of Energy Vehicle Technologies Program, *Battery Test Manual For Plug-In Hybrid Electric Vehicles*, Tech. rep. INL/EXT-07-12536, U.S. Department of Energy, Ch. 1 (2010).
2. M. Broussely, in *Advances in Lithium-Ion Batteries*, W. A. van Schalkwijk and B. Scrosati, Eds., Kluwer Academic, New York NY, Ch. 13 (2002).
3. L. Christodoulou and J. D. Venables, *Jom – Journal of the Minerals Metals & Materials Society*, **55**, 39 (2003).
4. O. Bitsche and G. Gutmann, *Journal of Power Sources*, **127**, 8 (2004).
5. Y. Xing, E. W. M. Ma, K. L. Tsui and M. Pecht, *Energies*, **4**, 1840 (2011).
6. W. A. van Schalkwijk, in *Advances in Lithium-Ion Batteries*, W. A. van Schalkwijk and B. Scrosati, Eds., Kluwer Academic, New York NY, Ch. 15 (2002).
7. T. Reddy and D. Linden, Eds., *Linden's Handbook of Batteries, 4th edition.*, McGraw-Hill, USA, Ch. 1 and Ch. 26 (2010).
8. P. Arora, R. E. White and M. Doyle, *Journal of the Electrochemical Society*, **145**, 3647 (1998).
9. J. Vetter, P. Novak, M. R. Wagner, C. Veit, K. C. Moller, J. O. Besenhard, M. Winter, M. Wohlfahrt-Mehrens, C. Vogler and A. Hammouche, *Journal of Power Sources*, **147**, 269 (2005).
10. D. P. Abraham, E. M. Reynolds, E. Sammann, A. N. Jansen and D. W. Dees, *Electrochimica Acta*, **51**, 502 (2005).
11. J. Shim and K. A. Striebel, *Journal of Power Sources*, **119**, 955 (2003).
12. M. Dubarry and B. Y. Liaw, *Journal of Power Sources*, **194**, 541 (2009).
13. K. Striebel, J. Shim, A. Sierra, H. Yang, X. Y. Song, R. Kostecki and K. McCarthy, *Journal of Power Sources*, **146**, 33 (2005).

14. P. Liu, J. Wang, J. Hicks-Garner, E. Sherman, S. Soukiazian, M. Verbrugge, H. Tataria, J. Musser and P. Finamore, *Journal of the Electrochemical Society*, **157**, A499 (2010).

15. J. Wang, S. Soukiazian, M. Verbrugge, H. Tataria, D. Coates, D. Hall and P. Liu, *Journal of Power Sources*, **196**, 5966 (2011).

16. M. Safari and C. Delacourt, *Journal of the Electrochemical Society*, **158**, A1123 (2011).

17. M. Kassem, J. Bernard, R. Revel, S. Pelissier, F. Duclaud and C. Delacourt, *Journal of Power Sources*, **208**, 296 (2012).

18. H. Zheng, L. Chai, X. Song and V. Battaglia, *Electrochimica Acta*, **62**, 256 (2012).

19. G. Gachot, S. Grugeon, M. Armand, S. Pilard, P. Guenot, J.-M. Tarascon and S. Laruelle, *Journal of Power Sources*, **178**, 409 (2008).

20. S. E. Sloop, J. B. Kerr and K. Kinoshita, *Journal of Power Sources*, **119**, 330 (2003).

21. A. J. Smith, H. M. Dahn, J. C. Burns and J. R. Dahn, *Journal of the Electrochemical Society*, **159**, A705 (2012).

22. Y. C. Zhang, C. Y. Wang and X. D. Tang, *Journal of Power Sources*, **196**, 1513 (2011).

23. S. C. Nagpure, B. Bhushan, S. Babu and G. Rizzoni, *Scripta Materialia*, **60**, 933 (2009).

24. D. P. Abraham, J. Liu, C. H. Chen, Y. E. Hyung, M. Stoll, N. Elsen, S. MacLaren, R. Twesten, R. Haasch, E. Sammann, I. Petrov, K. Amine and G. Henriksen, *Journal of Power Sources*, **119**, 511 (2003).

25. E. Peled and D. Golodnitsky, in *Lithium-Ion Batteries : Solid-Electrolyte Interphase*, B. P. Balbuena and Y. Wang, Eds, Imperial College Press, London UK, Ch.1 (2003).

26. L. Yang, M. Takahashi and B. F. Wang, *Electrochimica Acta*, **51**, 3228 (2006).

27. M. Koltypin, D. Aurbach, L. Nazar and B. Ellis, *Electrochemical and Solid State Letters*, **10**, A40 (2007).

28. K. Amine, J. Liu and I. Belharouak, *Electrochemistry Communications*, **7**, 669 (2005).

29. N. Dupré, J.-F. Martin, J. Degryse, V. Fernandez, P. Soudan and D. Guyomard, *Journal of Power Sources*, **195**, 7415 (2010).

30. M. Maccario, L. Croguennec, F. Le Cras and C. Delmas, *Journal of Power Sources*, **183**, 411 (2008).

31. A. M. Andersson and K. Edström, *Journal of the Electrochemical Society*, **148**, A1100 (2001).

32. L. Castro, R. Dedryvere, J. B. Ledeuil, J. Breger, C. Tessier and D. Gonbeau, *Journal of the Electrochemical Society*, **159**, A357 (2012).

33. M. Broussely, P. Biensan, F. Bonhomme, P. Blanchard, S. Herreyre, K. Nechev and R. J. Staniewicz, *Journal of Power Sources*, **146**, 90 (2005).

34. S. Ramdon and B. Bhushan, *Journal of Colloid and Interface Science*, **380** (2012).

35. X. Zhang, P. N. Ross, R. Kostecki, F. Kong, S. Sloop, J. B. Kerr, K. Striebel, E. J. Cairns and F. McLarnon, *Journal of the Electrochemical Society*, **148**, A463 (2001).

36. D. Dees, E. Gunen, D. Abraham, A. Jansen and J. Prakash, *Journal of the Electrochemical Society*, **155**, A603 (2008).

37. M. Kerlau, M. Marcinek, V. Srinivasan and R. M. Kostecki, *Electrochimica Acta*, **52**, 5422 (2007).

38. M. Dubarry, B. Y. Liaw, M.-S. Chen, S.-S. Chyan, K.-C. Han, W.-T. Sie and S.-H. Wu, *Journal of Power Sources*, **196**, 3420 (2011).

39. M. Safari and C. Delacourt, *Journal of the Electrochemical Society*, **158**, A1436 (2011).

40. L. Norin, R. Kostecki and F. McLarnon, *Electrochemical and Solid State Letters*, **5**, A67 (2002).

41. R. Kostecki, L. Norin, X. Y. Song and F. McLarnon, *Journal of the Electrochemical Society*, **151**, A522 (2004).

42. K. Amine, C. H. Chen, J. Liu, M. Hammond, A. Jansen, D. Dees, I. Bloom, D. Vissers and G. Henriksen, *Journal of Power Sources*, **97-8**, 684 (2001).

43. S. Brown, N. Mellgren, M. Vynnycky and G. Lindbergh, *Journal of the Electrochemical Society*, **155**, A320 (2008).

44. Y. Itou and Y. Ukyo, *Journal of Power Sources*, **146** (2005).

45. Y. T. Cheng and M. W. Verbrugge, *Journal of the Electrochemical Society*, **157**, A508 (2010).

46. M. W. Verbrugge and Y. T. Cheng, *Journal of the Electrochemical Society*, **156**, A927 (2009).

47. K. Striebel, J. Shim, A. Sierra, H. Yang, X. Y. Song, R. Kostecki and K. McCarthy, *Journal of Power Sources*, **146** (2005).

48. D. Y. Wang, X. D. Wu, Z. X. Wang and L. Q. Chen, *Journal of Power Sources*, **140**, 125 (2005).

49. C. Peabody and C. B. Arnold, *Journal of Power Sources*, **196**, 8147 (2011).

50. J.-i. Yamaki, in *Advances in Lithium-Ion Batteries*, W. A. van Schalkwijk and B. Scrosati, Eds., Kluwer Academic, New York NY, Ch. 5 (2002).

51. Z. Ogumi and M. Inaba, in *Advances in Lithium-Ion Batteries*, W. A. van Schalkwijk and B. Scrosati, Eds., Kluwer Academic, New York NY, Ch. 2 (2002).

52. N. A. Kaskhedikar and J. Maier, *Advanced Materials*, **21**, 2664 (2009).

53. J.-P. Issi and B. Nysten, in *Carbon fibres, 3rd edition*, J. B. Donnet and R. C. Bansal, Eds., Marcel Dekker Inc., New York NY, Ch. 6 (1998).

54. H. O. Pierson, *Handbook of Carbon, Graphite, Diamond and Fullerenes - Properties, Processing and Applications*, William Andrew Publishing, Park Ridge NJ, Ch. 8 (1993).

55. D. D. Edie and J. J. McHugh, in *Carbon Materials for Advanced Technologies*, T. D. Burchell, Eds., Elsevier Science Ltd, Oxford UK, Ch. 4, (1999).

56. X. Huang, *Materials*, **2**, 2369 (2009).

57. N. Imanishi, H. Kashiwagi, T. Ichikawa, Y. Takeda, O. Yamamoto and M. Inagaki, *Journal of the Electrochemical Society*, **140**, 315 (1993).

58. K. Suzuki, T. Iijima and M. Wakihara, *Electrochimica Acta*, **44**, 2185 (1999).

59. T. Iijima, K. Suzuki and Y. Matsuda, *Synthetic Metals*, **73**, 9 (1995).

60. J. F. Snyder, E. L. Wong and C. W. Hubbard, *Journal of the Electrochemical Society*, **156**, A215 (2009).

61. J. K. Lee, K. W. An, J. B. Ju, B. W. Cho, W. I. Cho, D. Park and K. S. Yun, *Carbon*, **39**, 1299 (2001).

62. R. Kanno, Y. Kawamoto, Y. Takeda, S. Ohashi, N. Imanishi and O. Yamamoto, *Journal of the Electrochemical Society*, **139**, 3397 (1992).

63. H. Zhang, S. Kulkarni and S. L. Wunder, *Journal of Physical Chemistry B*, **111**, 3583 (2007).

64. L. Cokbaglan, N. Arsu, Y. Yagci, S. Jockusch and N. J. Turro, *Macromolecules*, **36**, 2649 (2003).

65. C. Gerbaldi, J. R. Nair, S. Ahmad, G. Meligrana, R. Bongiovanni, S. Bodoardo and N. Penazzi, *Journal of Power Sources*, **195**, 1706 (2010).

66. J. F. Snyder, E. D. Wetzel and C. M. Watson, *Polymer*, **50**, 4906 (2009).

67. M. Willgert, M. H. Kjell, E. Jacques, M. Behm, G. Lindbergh and M. Johansson, *European Polymer Journal*, **47**, 2372 (2011).

68. B. Scrosati, in *Advances in Lithium-Ion Batteries*, W. A. van Schalkwijk and B. Scrosati, Eds., Kluwer Academic, New York NY, Ch. 8 (2002).

69. J. P. Thomas and M. A. Qidwai, *Acta Materialia*, **52**, 2155 (2004).

70. J. P. Thomas and M. A. Qidwai, *Jom – Journal of the Minerals Metals & Materials Society*, **57**, 18 (2005).

71. J. F. Snyder, R. H. Carter, E. L. Wong, P.-A. Nguyen, E. H. Ngo and E. D. Wetzel, *Proceedings of the 25th Army Science Conference*, Orlando FL 27-30 November (2006).

72. E. L. Wong, D. M. Baechle, K. Xu, R. H. Carter, J. F. Snyder and E. D. Wetzel, *Proceedings of Society for the Advancement of Materiel and Process Engineering (SAMPE)*, Baltimore MD 3-7 June (2007).

73. P. Liu, E. Sherman and A. Jacobsen, *Journal of Power Sources*, **189**, 646 (2009).

74. S. Ekstedt, M. Wysocki and L. E. Asp, *Plastics Rubber and Composites*, **39**, 148 (2010).

75. A. K. Padhi, K. S. Nanjundaswamy and J. B. Goodenough, *Journal of the Electrochemical Society*, **144** (1997).

76. *Electrically propelled road vehicles – Test specifications for lithium-ion traction battery packs and systems – Part 1: High-power applications*, ISO 12405-1 (2011).

77. A. Nyman, T. G. Zavalis, R. Elger, M. Behm and G. Lindbergh, *Journal of the Electrochemical Society*, **157**, A1236 (2010).

78. M. Herstedt, D. P. Abraham, J. B. Kerr and K. Edström, *Electrochimica Acta*, **49**, 5097 (2004).

79. D. D. MacNeil, D. Larcher and J. R. Dahn, *Journal of the Electrochemical Society*, **146**, 3596 (1999).

80. M. N. Richard and J. R. Dahn, *Journal of the Electrochemical Society*, **146**, 2068 (1999).

81. S. S. Zhang, *Journal of Power Sources*, **162**, 1379 (2006).

82. S. Brown, *Diagnosis of the Lifetime Performance Degradation of Lithium-Ion Batteries: Focus on Power-Assist Hybrid Electric Vehicle and Low-Earth-Orbit Satellite Applications*, Ph.D. Thesis, KTH Royal Institute of Technology, Stockholm Sweden (2008).

83. K. R. Kganyago and P. E. Ngoepe, *Physical Review B*, **68** (2003).

84. Y. Qi, H. Guo, L. G. Hector, Jr. and A. Timmons, *Journal of the Electrochemical Society*, **157**, A558 (2010).

85. D. D. Edie, *Carbon*, **36**, 345 (1998).